Soils and Rocks
An International Journal of Geotechnical and Geoenvironmental Engineering
www.soilsandrocks.com
ISSN 1980-9743
ISSN-e 2675-5475

Nonlinear modeling of high-performance fiber-reinforced concrete in tunnels: evaluation through field and laboratory testing

Tiago de Jesus Souza[1#], David Oliveira[2]

Case Study

Keywords
Yield line
Segments
Fibre-reinforced concrete
Numerical simulation

Abstract

The design of fibre-reinforced concrete structures must follow the design principles concerning limit states, similar to those adopted for conventionally reinforced concrete. However, the use of linear elastic analysis or conventional yield-line theory may, in many cases, underestimate the benefits of fibres in providing greater load-bearing capacity, particularly when high-performance steel fibres are adopted. This paper presents two case studies of real tunnel projects in which the author was involved, where the use of non-linear modelling of steel fibre-reinforced concrete elements, coupled with physical testing, provided significant benefits in the design and construction of tunnel linings. The first case focuses on the design of thin tunnelling linings using rock-bolted shotcrete. In this case, the non-linear modelling coupled with full-scale field tests demonstrated load-bearing capacities up to 6-7x greater than conventional design methods. The second case presents the design of a segment lining and the effects of fibre reinforcement on the bursting and splitting capacity of longitudinal joints under rotation. In this case, non-linear modelling coupled with laboratory testing on large-scale segment joint samples demonstrated that conventional reinforcement was unnecessary, whereas analysis with linear-elastic theory indicated otherwise.

1. Introduction

Concrete is inherently strong in compression but weak in tension, exhibiting brittle behaviour under typical unconfined conditions. To address these limitations, steel reinforcement bars are traditionally used to resist tensile forces after cracking, thereby enhancing the ductility of the structural system. In conventional reinforced concrete, the tensile strain at which concrete cracks is significantly lower than the yield strain of steel, meaning that cracking occurs before substantial load transfer to the reinforcement. Consequently, steel bars also serve to control crack widths, ensuring serviceability, aesthetics, and, critically, long-term durability.

Fibre reinforcement in concrete seeks to achieve similar objectives: providing post-crack tensile and flexural capacity while limiting crack widths. Unlike discrete reinforcing bars, fibres are uniformly dispersed throughout the concrete volume, resulting in a much smaller spacing between reinforcement elements. This transforms the system from a two-material assembly into a composite material. This conceptual shift is essential for design, as conventional reinforced concrete approaches may not fully capture the performance advantages of fibre-reinforced concrete (FRC), a topic further explored in this paper.

One of the main advantages of using fibre-reinforced concrete is its ability to significantly reduce construction time compared to traditional methods that rely on single or double layers of steel bars or welded wire mesh. This is achieved by eliminating the need for heavy equipment to lift and place reinforcement cages, as FRC can be directly pumped or sprayed into place. Such simplification can save several weeks on large-scale tunnel projects. Additionally, reducing labour-intensive activities enhances jobsite safety by minimising the number of personnel required and their exposure to high-risk environments, particularly when working at height.

However, due to fresh concrete workability requirements and the need for uniform fibre distribution during mixing, there are practical limits to the amount of steel fibres that can be incorporated into the concrete mix. Consequently, the structural capacity of fibre-reinforced concrete may not match that of conventionally reinforced concrete. Despite this limitation, designers and contractors often seek structural efficiencies by reducing member sizes, such as lining thickness, which can be achieved when higher capacity FRC mixtures are used. These reductions lead to lower concrete volumes, directly decreasing formwork requirements for cast-in-situ linings and minimizing both the cost and risks associated with the transportation of tunnel boring machine (TBM) segments, as well as overall concreting time.

[#]Corresponding author. E-mail address: tiagosouza@ufscar.br
[1]Universidade Federal de São Carlos, Departamento de Engenharia Civil, São Carlos, SP, Brasil.
[2]Aurecon, Tunnel Department, Brisbane, QLD, Australia.

Submitted on July 21, 2025; Final Acceptance on January 8, 2026; Discussion open until August 31, 2026.
Editor: Renato P. Cunha
https://doi.org/10.28927/SR.2026.011325

High-performance fibres aim to address two fibre-reinforcement mechanisms: fibre pull-out and fibre yielding/rupture (Figure 1). A good fibre-concrete bond is essential for developing post-cracking tensile capacity across the crack. High ductility FRC is obtained when fibres are pulled out across cracks in a controlled manner without significant yield or rupture.

However, it is essential to understand the difference between ductility and toughness. Ductility is the ability of the material to develop relatively large deformations before rupturing. Conversely, toughness is the material's resistance to large deformations, a combination of ductility and capacity. In most design cases, high toughness is the target, and the fibre yield capacity must be compatible with the pull-out capacity to achieve high toughness. For this reason, developing high-performance fibres involves improvements in both pull-out and yield strength.

Figure 2 presents two examples of steel fibres used in shotcrete applications in Australia. The left-hand side is a traditional end-hooked steel fibre commonly used in tunnelling applications. The right-hand side is a high-performance version with "double" end hooks for better strength development, particularly at low deformation and small crack widths (≤ 0.5 mm). As seen, the improvement in pull-out capacity is followed by an increase in tensile strength from 1345 MPa to 1850 MPa. The high-performance steel fibre presented in Figure 2 is an improvement of an older but similar double-end hooked fibre version of the same supplier with a different aspect ratio and length (Dramix 4D 65/60BG). An increase in tensile strength from 1500 MPa to 1850 MPa was necessary to reduce the yielding of the fibres and achieve higher "toughness" values at crack widths exceeding 3 mm, i.e. at ultimate limit state, and when the smaller diameter version (65/35) was used with concretes with average compressive strengths, f_{cm}, greater than 50 MPa.

With high-capacity steel fibres now available, there is a natural desire to leverage their use in design, potentially reducing tunnel lining thickness or replacing conventional steel bar reinforcement where possible, due to the abovementioned advantages. Such a design reduces construction costs and can provide more sustainable solutions with a lower carbon footprint by reducing the volume of concrete used and the quantity of steel.

This paper presents two case studies of tunnel projects in Australia in which high-performance steel fibres were adopted in the design and verified through testing, resulting in significant project benefits. The first case refers to a shotcrete application, whilst the second is a pre-cast segmental lining design.

2. Case studies from Sydney, Australia

2.1 Geotechnical conditions

Tunnelling works in the Sydney region relate largely to Triassic sandstones and shales that underlie most of the metropolitan area. The Hawkesbury Sandstone formation

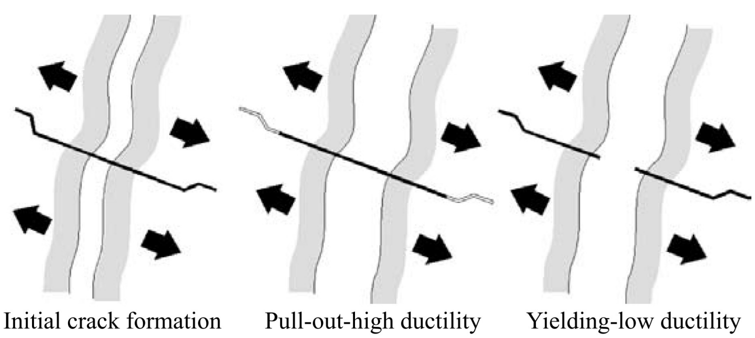

Figure 1. Fibre behaviour (Bernard, 2008).

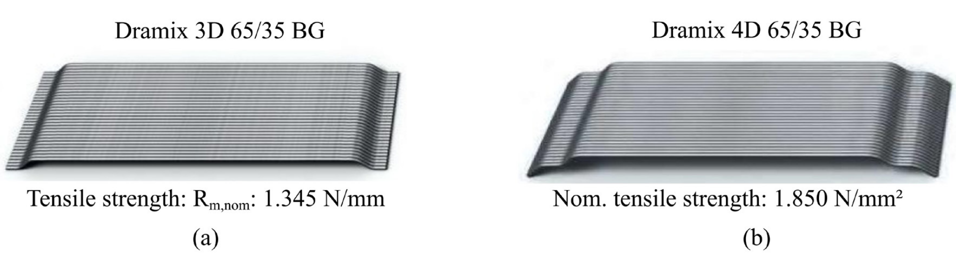

Figure 2. Examples of end-hooked steel fibres: (a) more traditional fibre on the left-hand side; (b) high- performance "double-end-hooked" fibre on the right-hand side.

tends to dominate the Sydney region, both in engineering structures and in natural topography. When viewed in a vertical section, Hawkesbury Sandstone may be divided into three facies, namely: sheet facies, massive facies (these two make up 95% of the formation), and mudstone facies (5% of the formation). In general, tunnelling conditions in Hawkesbury Sandstone are relatively favourable, despite the very high stresses experienced in Sydney, with the horizontal-to-vertical stress ratio regularly exceeding k > 3. The typical uniaxial compressive strength of Hawkesbury Sandstone is above 12 MPa, with rock mass quality ranging from poor to very good, with *Q-values* mostly above 1 and RMR values above 40, although all of these values can be locally lower at faults and shear zones and in shallow conditions.

2.2 Shotcrete application on M4-M8 link tunnels

For conventionally mined tunnels in poor to fair-quality rock masses (i.e., with *Q-values* between 0.4 and 10), global stability and ground support can still be achieved primarily through ground reinforcement, such as rock bolts. Such reinforcement elements not only hold unstable rock wedges and blocks but also provide local shear and tensile reinforcement where they cross rock defects or discontinuities, enhancing the rock mass's capacity to redistribute stresses during tunnel excavation more safely. However, rock bolt spacing needs to be kept cost-effective, and as such, the use of some surface retention system, such as shotcrete, is still necessary to promote local stability and stress arching (Figure 3a). In these cases, the shotcrete is locally supported by the rock bolts, and it is often designed to span the loads between them against both flexural and punching failure mechanisms (Figure 3a and Figure 3b).

At the start of construction of the Westconnex motorway project in Sydney, both the New M4 and M8 tunnels included in their shotcrete specifications the intention to achieve a high-performance Fibre-Reinforced Shotcrete (FRS). This intention was expressed by specifying relatively high design values for residual flexural strengths at SLS and (ULS), respectively: $f_{R1} = 3.5$ MPa and $f_{R4} = 3.0$ MPa, in accordance with BS 14651. These values could be considered relatively common practice in cast-in-situ applications at the time of construction of these projects, using longer, larger-diameter fibres, but, to the author's knowledge, less common in sprayed concrete (shotcrete), where shorter, smaller-diameter fibres are generally preferred due to workability.

These projects adopted the steel fibre shown on the left-hand side of Figure 2 in their mix design with a fibre count of 40-45 kg/m^3 and a 40 MPa concrete strength. The performance during production indicated that the specified values of $f_{R1} = 3.5$ MPa and $f_{R4} = 3.0$ MPa were achieved only as average values, i.e., not as 95% characteristic, resulting in approximately 50% of non-conformances that had to be addressed via the project's NCR process.

The M4-M8 Link Tunnels were the next project to be constructed as part of the Westconnex motorway. Despite the unsuccessful previous attempt, this project took on the challenge of achieving high performance since the residual flexural strength values of the New M4 and M8 tunnels were incorporated into the project's Scope of Works and Technical Criteria (SWTC).

The design team then recommended using the high-performance fibre shown on the right-hand side of Figure 2 as the world's first shotcrete application with such fibres, which was taken forward by the construction and procurement teams, resulting in a shotcrete mix design that performed as

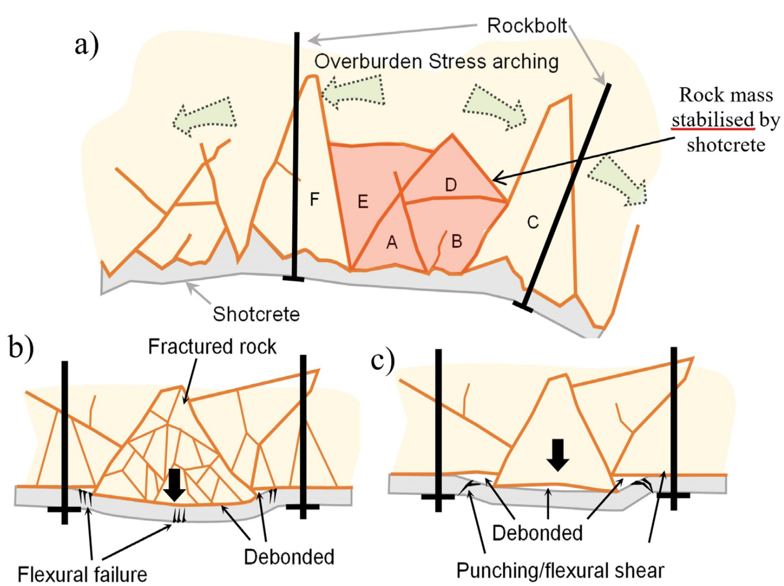

Figure 3. (a) Concept of local stability promoted by combined shotcrete and rock bolts; (b) Flexural failure mechanisms and (c) Punching or flexural shear failure mechanisms (Oliveira, 2020).

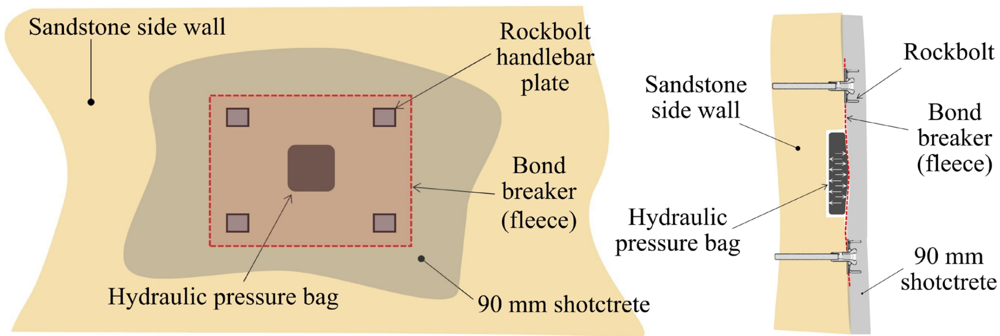

Figure 4. Schematic of large-scale field testing on shotcrete lining.

Figure 5. Photos of the large-scale field testing on shotcrete lining.

intended during construction, i.e., with characteristic values of f_{R1k} = 3.5 MPa and f_{R4k} = 3.0 MPa, and a minimal number of non-conformances. Following the successful mix design, the next question was: how to leverage such a high-performance Steel Fibre-Reinforced Shotcrete (SFRS) in tunnel lining design?

An investigation into pushing the boundaries of the flexural capacity of thin, rock-bolted shotcrete linings led the design team to consider compressive membrane action (CMA) in the structural performance of the tunnel linings. Non-linear stress analysis investigations during the detailed design stage provided confidence that such an approach could give the linings a capacity many times greater than conventionally predicted in the past with either deterministic methods, such as Barrett & McCreath (1995) or yield line theory.

The design team proposed large-scale field tests of the as-constructed shotcrete linings, 90 mm thick, to confirm the significant benefits, following verification assisted by testing (FIB, 2013). A schematic of the test, using hydraulic bags to load the shotcrete lining to failure, is depicted in Figure 4, with representative photographs shown in Figure 5. Further details are presented in Bernard et al. (2022).

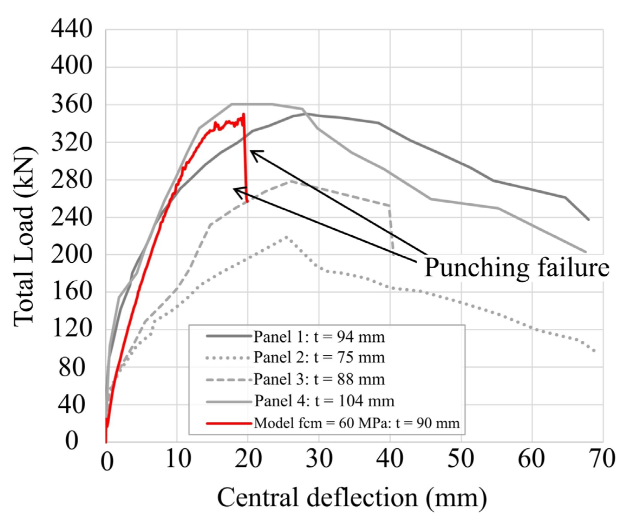

Figure 6. Large-scale field test results with numerical back-analysis.

The test results are presented in Figure 6 against the predictions of a numerical back-analysis conducted after the tests.

The back-analysis followed the same methodology described in Bernard et al. (2022) but now incorporated the actual rock bolt plate geometry embedded into the shotcrete, modelled as presented by Oliveira & Kozak (2021).

All four test panels indicated a load capacity approximately 4-5 times greater than that predicted by conventional methods used in previous projects, about 65 kN for a 90 mm thick lining. In addition, visual inspections of the failed panels during testing and the numerical back-analysis model confirmed that the capacity of the 90 mm thick lining was mainly limited by the pull-out capacity or punching shear failure of the rock bolts, as shown in Figure 7, also highlighted by the yielding of the handlebars. Once the four rock bolt plates forming the shotcrete panel failed (pulled out), the shotcrete lining would span further to the neighbouring rock bolts. As a result, the ductility seen in Figure 6 post-peak behaviour resulted from the enhanced flexural capacity provided by the high-performance steel fibres, allowing the lining panels to tolerate the significant increase in span. In contrast, the numerical back-analysis model shows brittle failure during rock bolt pull-out, as it considers only one-quarter of the geometry and assumes symmetry at the four sides of the model, leading to all neighbouring bolts failing as well. Nevertheless, the numerical back-analysis confirmed that lining capacity was limited by the punching shear of the bolts rather than a flexural failure of the lining.

The above application of high-performance steel fibres in shotcrete allowed a reduction of approximately 15% in tunnel lining thickness with the following additional outcomes:

- The project benefited from a reduction of more than 33,000 tons of embodied carbon (CO_{2e}) from the reduced amount of shotcrete used on the project by 27,000m^3 (15%) and reinforced steel fibres by 830 tonnes (10%).
- Approximately 9,000 heavy vehicle movements were removed from Sydney's local and main roads as less shotcrete was required to be supplied.
- The project demonstrated cost savings of $11,000,000 by minimising materials by applying the innovative high-performance shotcrete.

The second case study presented in this paper refers to the design of TBM segment joints for a metro project in Sydney, as discussed below.

2.3 Enhanced bursting/splitting capacity for TBM segment joints

The design action effects, essentially bending moments and axial forces, acting on the segmental lining need to be transferred between segments in a ring via the performance of their joints, particularly the longitudinal or radial joints. These actions are transferred by simple compression, where the applicable eccentricity induces joint rotation due to bending moments acting on the segment bodies or additional distortions from geometrical ring build imperfections. This becomes particularly relevant in cases of soft ground tunnelling and/or high hydrostatic stresses, which, when combined with construction tolerances, can subject tunnel segments to high levels of rotation and highly concentrated stresses/forces.

The immediate failure mechanism associated with joint compression is simple bearing crushing. However, this simple compression and its associated deformed shape generate tension at a certain depth, as illustrated in Figure 8a. Suppose the section is hypothetically split vertically into two along the centre axis of the applied load. In that case, it is straightforward to visualise that the top zone of the two sections tends to form a bowl under the loads, thus deforming inward transversely. In contrast, the deeper area of the two sections tends to move and rotate transversely outward. As a result, the start of the section tends to go into compression, while the deeper section is in tension, with an associated potential for bursting/splitting failure. This behaviour is also confirmed by the elastic analyses conducted by Iyengar (1962), as depicted in Figure 8b.

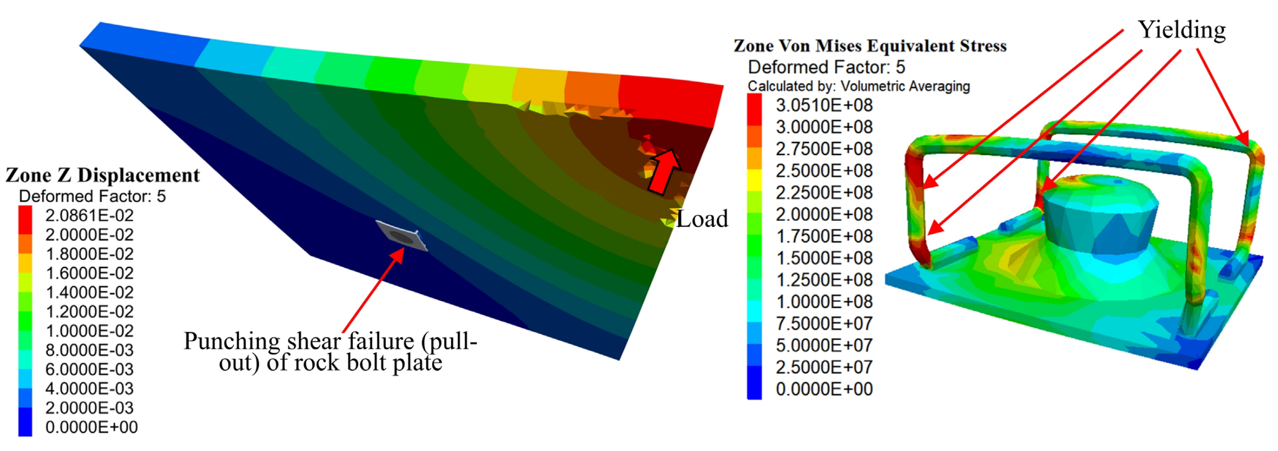

Figure 7. Numerical back-analysis of one-quarter of the panel.

The typical design of longitudinal joints often involves analysing the applicable elastic stresses acting in the potential bursting zone within the disturbed region (*D-region*), either through numerical analysis or using an approximate solution proposed by Iyengar (1962). Suppose the maximum tensile stress in the *D-region* is estimated to be lower than the design splitting strength of the FRC segment, which is the peak tensile splitting strength reduced by a safety factor. In that case, the design is deemed satisfactory without further reinforcement requirements based on the assumption that the risk of cracking initiation parallel to the applied load is mitigated and that the fibre reinforcement controls any minor preexisting cracking. On the other hand, if the maximum tensile strength is exceeded, additional checks assuming the residual tensile strength of the FRC are required or additional conventional bar reinforcement must be added.

If the residual tensile capacity of the FRC is to be used in the design without bar reinforcement, analysis of joints with concentrated loads will often follow the classic strut-and-tie model proposed by Leonhardt & Mönnig (1973). The diffusion of transverse stresses is assumed to develop within the *D-region*, which is assumed to be limited to the segment thickness (*d* or *h*) or the effective thickness (d_l or *'h-2e'*), as shown in Figure 8b. The tensile transverse stresses are uniformly distributed over a length of 0.8*h*, while compression is distributed along 0.2*h*, as depicted in Figure 9 and Equation 1.

$$\text{Tie force, } T = 0.25F_d\left(1-\frac{h_1}{h-2e}\right) \tag{1}$$

Design analysis for a section of the Sydney Metro approaching depths of 90 m and with high groundwater pressures indicated that the longitudinal joints of the 260 mm thick segments (with a joint length of 130 mm) could experience axial forces of up to 4000 kN/m at ULS, i.e. already factored up, with an eccentricity of up to 30 mm (Figure 10) including geometrical ring build imperfections. This load can be applied as an equivalent rectangular stress block with a length of 50 mm.

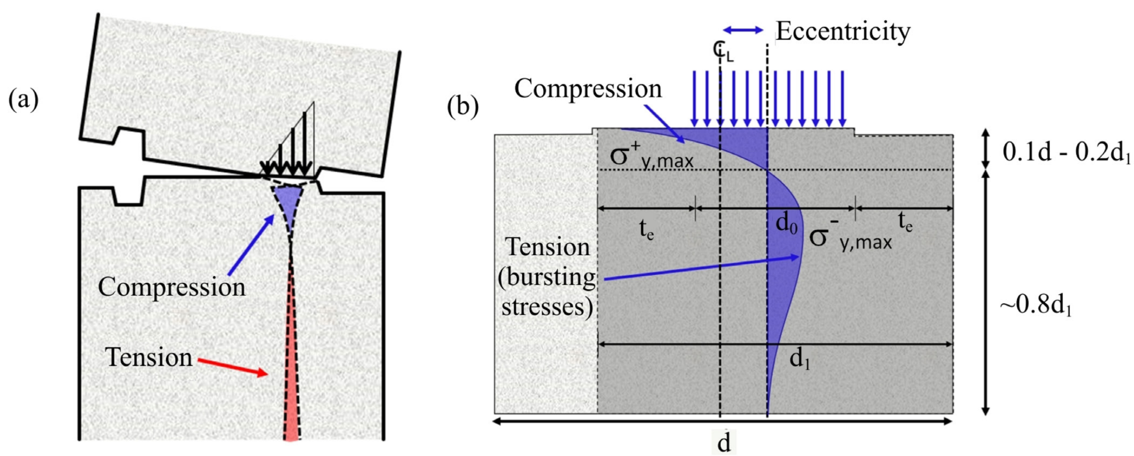

Figure 8. (a) Conceptual behaviour of joint compression; (b) Distribution of transverse stresses along the equivalent centre axis of loads (Harding, 2022).

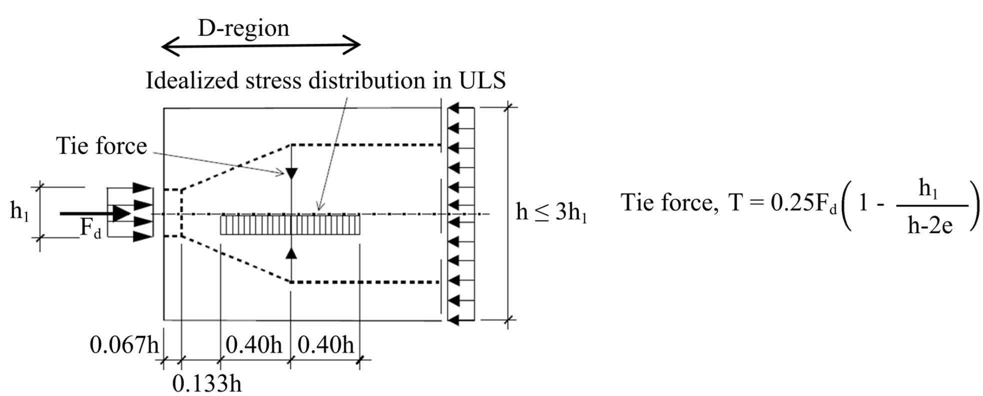

Figure 9. Strut-and-tie model to design partially loaded areas (DAfStb Stahlfaserbeton, 2010).

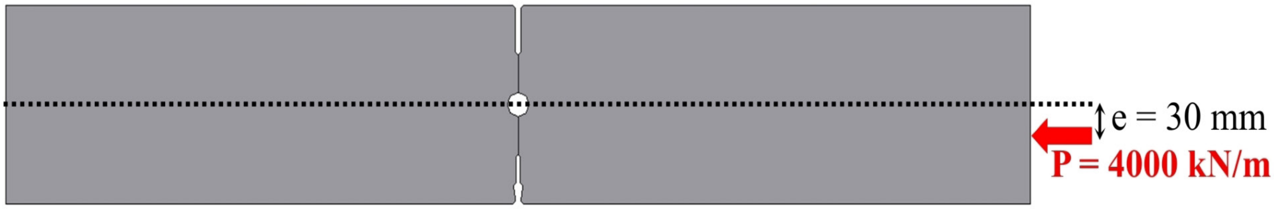

Figure 10. Critical joint load case for segmental lining design.

A tie force T = 750 kN/m can be estimated based on the Equation 1, taking F_d = 4000 kN/m, h_1 = 50 mm, h = 260 mm and e = 30 mm. The design capacity, R, to resist such tensile force is estimated by multiplying the tensile residual strength of the FRC by the length of 0.8(h-2e) and then factored down by a typical reduction factor of 0.6. The design capacity was estimated as R = 151 kN/m based on a typical residual tensile strength of 1.575 MPa for an associated f_{R1} = 3.5 MPa for FRC mixes using the Dramix 4D 80/60 BG fibre (tensile strength of 1800 MPa).

The above-estimated design capacity is significantly below the design tie force, indicating a splitting failure that would, in principle, require extra bar reinforcement. However, there is a significant drawback in the assumption presented above. The assumed *D-region* is based on elastic solutions that ignore the beneficial effects of fibre reinforcement, which allow controlled crack propagation and are likely to increase the depth of the *D-region* significantly. As a result, the design team adopted the following steps to investigate the actual capacity of an FRC segment:

- Increase the residual tensile capacity of segments by using high-performance steel fibres. The previously used Dramix 4D 80/60 BG fibre, with a tensile strength of 1800 MPa, was replaced by the newer Dramix 4D 80/60 BGP with a tensile strength of 2200 MPa. The concrete mix design targeted f_{ck} = 66 MPa with f_{R1k} > 4 MPa and f_{R4k} > 4 MPa, achieved without increasing the fibre count compared to the previous fibre type.
- The design would be based on non-linear stress analysis to more accurately estimate crack propagation and strength development resulting from fibre reinforcement. It is important to note that the Model Code 2010 (FIB, 2013), Sections 7.2.2.4.4 and 7.11, and the AS 5100.5, Section 2.3.6, recommend that the mean values of the material characteristics be considered in such analysis.
- The design would also follow the verification assisted by testing principles described in section 7.12 of the Model Code 2010 (FIB, 2013) based on a combination with the non-linear model previously described. Verification assisted by testing is the procedure where loading tests on a limited series of representative specimens are used to determine the response of structural members or systems. The verification assisted by testing aims to obtain design values for the parameters governing the response of structural members and systems under specified load conditions for a certain limit state, in this case, splitting/bursting failure.

3. Non-linear stress analysis

A smeared-crack constitutive model was adopted in the commercial software ATENA to model both splitting and crushing of concrete. The plasticity model for crushing is based on the triaxial failure surface of Menetrey & Willam (1995) given by Equation 2 and Equation 3.

$$F_{3P}^{p} = \left[\sqrt{1.5}\,\frac{\rho}{f_c'}\right]^2 + m\left[\frac{\rho}{\sqrt{6}f_c'}r(\theta,e) + \frac{\xi}{\sqrt{3}f_c'}\right] - c = 0 \quad (2)$$

$$m = 3\frac{f_c'^2 - f_t'^2}{f_c' f_t'}\frac{e}{e+1}, r(\theta,e) = \frac{4\left(1-e^2\right)cos^2\theta + \left(2e-1\right)^2}{2\left(1-e^2\right)cos\theta + \left(2e-1\right)\left[4\left(1-e^2\right)cos^2\theta + 5e^2 - 4e\right]^{\frac{1}{2}}} \quad (3)$$

The entire model can also be described with respect to the equivalent uniaxial stress-strain law as depicted in Figure 11a with the compression behaviour before peak following the Model Code Clause 7.2.3.1.3 (FIB, 2013) described in Equation 4.

$$\sigma_c^{ef} = f_c'^{ef}\frac{kx - x^2}{1 + \left(k-2\right)x}, x = \frac{\varepsilon}{\varepsilon_c}, k = \frac{E_o}{E_c} \quad (4)$$

The effects of biaxial enhancement are considered based on the relationship presented by Kupfer et al. (1969), illustrated in Figure 11b.

The above model was adjusted in the tensile zone to follow the constitutive tensile law proposed by the Model Code 2010 (FIB, 2013), as shown in Figure 12.

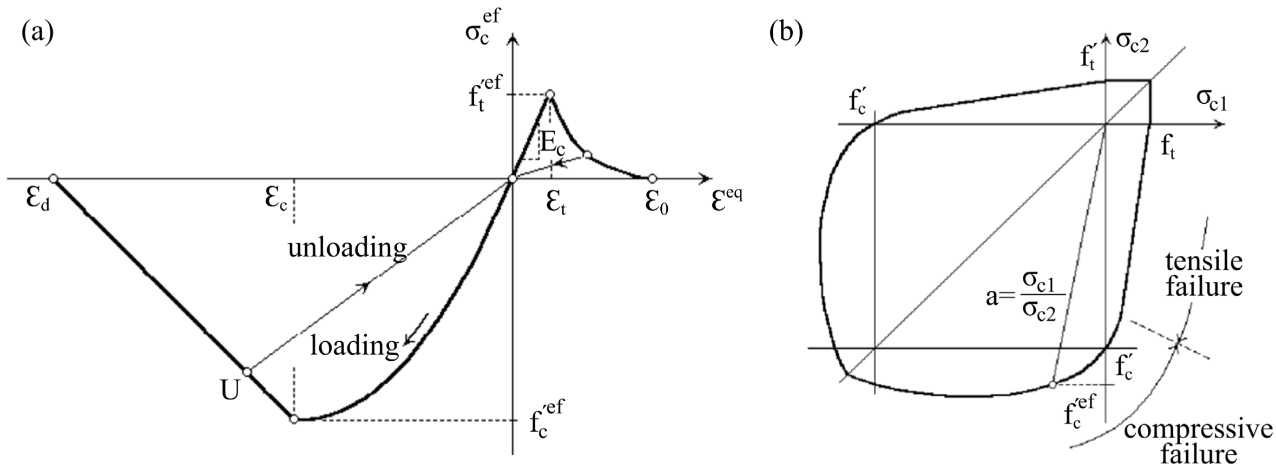

Figure 11. Concrete model: (a) Uniaxial stress-strain law (FIB, 2013); (b) Biaxial failure function (after Kupfer et al., 1969).

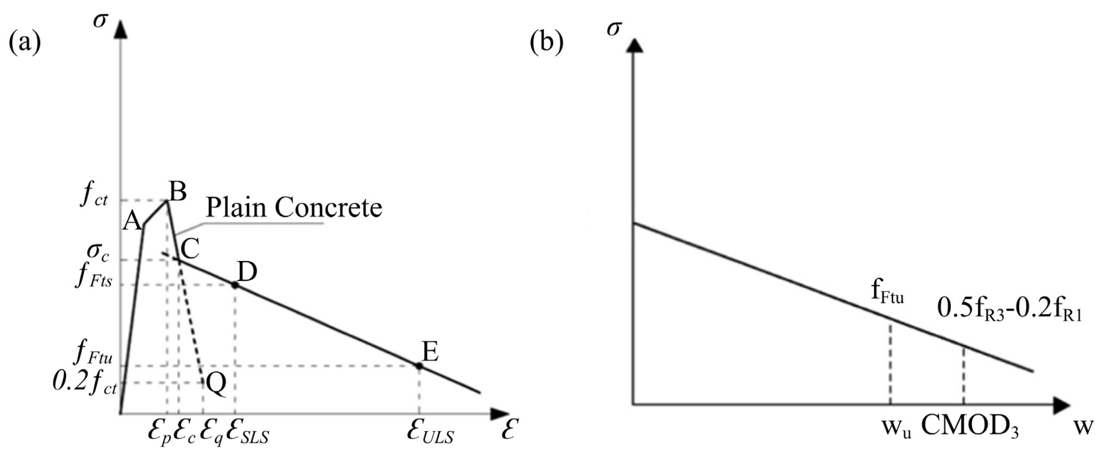

Figure 12. (a) Tensile constitutive law from Model Code 2010 (FIB, 2013); (b) corresponding crack width definitions.

The mix design pre-production testing indicated a value of f_{cm} = 75 MPa for the proposed f_{ck} = 66 MPa, which was also confirmed during production testing. The residual flexural tensile strengths previously discussed were converted to equivalent residual uniaxial tensile strength by the equivalent stress block factors of 0.45 and 0.37, respectively. The peak uniaxial tensile strength was adopted based on the targeted characteristic value estimated using equations provided in the Model Code 2010, resulting in f_{ctk} = 3.2 MPa; however, this underestimates the actual tensile strength, given a specified tensile splitting strength of 5 MPa for the mix. The Young Modulus was adopted as E = 37800 MPa.

Two partial segments, each 750 mm long, were modelled to represent the combined bending effects of the segments and the joint. The joint includes a guide rod pocket with a 32 mm diameter, and gasket and caulking grooves each 65 mm long. Considering that the segment depth is 260 mm, the contact length left for the longitudinal joints is 130 mm, of which 32 mm is the guide rod diameter/pocket. Contact elements were used between the segments with applied zero bond, i.e. zero tensile strength.

To achieve failure (i.e., collapse), the load is applied at an eccentricity of 30 mm on one side of the model, with the applied displacement incrementally increased to induce joint rotation.

Figure 13 presents the minor principal stresses, i.e. compressive stresses, developed at a joint rotation of 11.57 mrad. As observed, the stresses are distributed over the entire contact length on one side of the guide rod and approximately 15 mm on the other side, which, if converted to an equivalent uniformly distributed load, could be conservatively assumed to act only on one side of the rod, i.e. with a = 50 mm. The maximum crack width observed was approximately 0.6 mm with no signs of a wedge failure formation, i.e. punching shear of the stress block. Figure 14 shows the load rotation behaviour of the FRC joint with a peak resistance of approximately 6250 kN/m. A design resistance of 3810 kN/m is estimated if a reduction factor of 0.6 is applied to the predicted peak resistance.

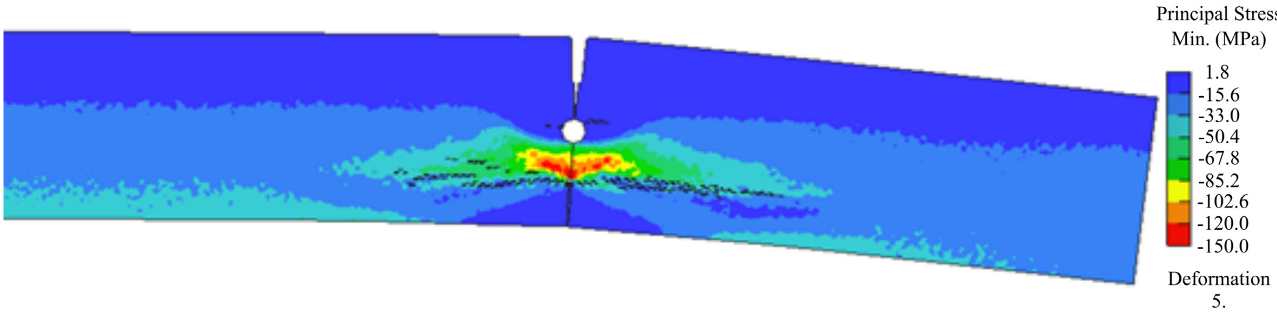

Figure 13. Minor principal stress (compression) distribution at peak capacity with a maximum observed crack width of approximately 0.5 mm.

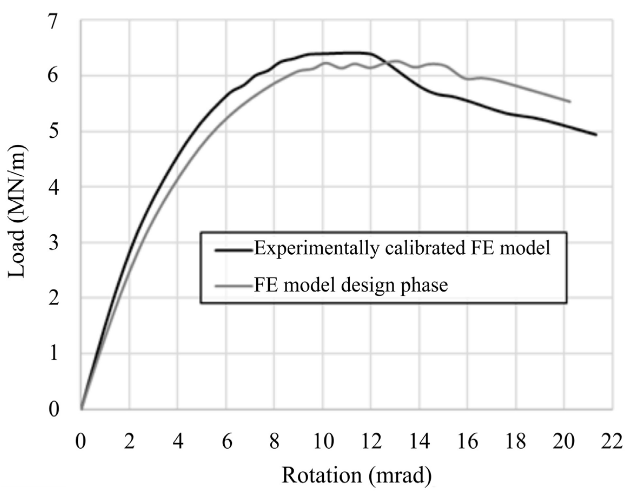

Figure 14. Model results for load-rotation performance.

Considering that it is only approximately 6% lower than the ULS load, i.e. already factored up, this capacity can be deemed acceptable if verified by testing due to increased confidence in the predictions.

4. Verification assisted by testing

Three specimens representative of segment joints were tested under concentrated loads to verify the above predictions of bursting and splitting. The joint samples were square columns measuring 260 mm x 260 mm x 650 mm and cast with the same concrete mix design as the segments. The top section of the columns was formed to have the same geometry as the segment longitudinal joints. The layout of the tests is depicted in Figure 15.

LVDT sensors were connected to one side of the samples and positioned against reference arms glued to the other side of the specimen (Figure 15 LHS) at several depths to monitor the lateral expansion and, consequently, the crack widths.

The specimens were loaded over the entire available joint area on one side of the guide rod, over a length of 50 mm (Figure 16). This configuration represents an eccentricity of 40 mm, which is more severe than the case previously discussed and, therefore, considered conservative for verification purposes.

Figure 16 presents the test results against a numerical back-analysis of the tests to calibrate the FRC parameters. Unfortunately, the compression machine used for testing was not servo-displacement-controlled, so it could not accurately capture the post-peak behaviour, as the test increments were based on load rather than displacement. Nevertheless, the most relevant phase of the tests up to peak resistance was adequately captured and could be used for comparison against model predictions. Post-peak performance could also be qualitatively assessed by comparing the cracking patterns observed in the samples and those observed in the numerical model (Figure 16 RHS).

As observed above, the back-analysis model reproduced the experimental results with high agreement on loads, crack widths, and lengths. It should be noted, however, that the model stopped at a crack width of 1.9 mm while the tests had crack widths up to 7 mm. An important observation of the verification tests is the cracks' development length and, therefore, the *D-region* depth. In all tests, the average length corresponded to approximately 2 to 2.7 times the effective thickness of 180 mm (i.e. 260-2*40). This observation confirmed the previous hypotheses that a *D-region* limited to 0.8(h-2e) is over-conservative and cannot adequately capture the benefits of the fibres.

Based on the test results alone, it could be estimated that a 1 m joint length would provide an ultimate capacity of 1600 kN x 1000 mm / 260 mm = 6150 kN/m. However, as highlighted above, these tests imposed a higher eccentricity and are therefore conservative, as the joint experiences greater rotations.

The material parameters adopted in the segment joint design analyses were recalibrated based on the current numerical back-analysis results as a final design check. The analysis discussed in the previous section was then re-run. Figure 14 presented the experimentally recalibrated curve with marginally higher predicted capacity, i.e. 6350 kN/m instead of the previous 6250 kN/m, indicating a good quality Class-A prediction during the design phase.

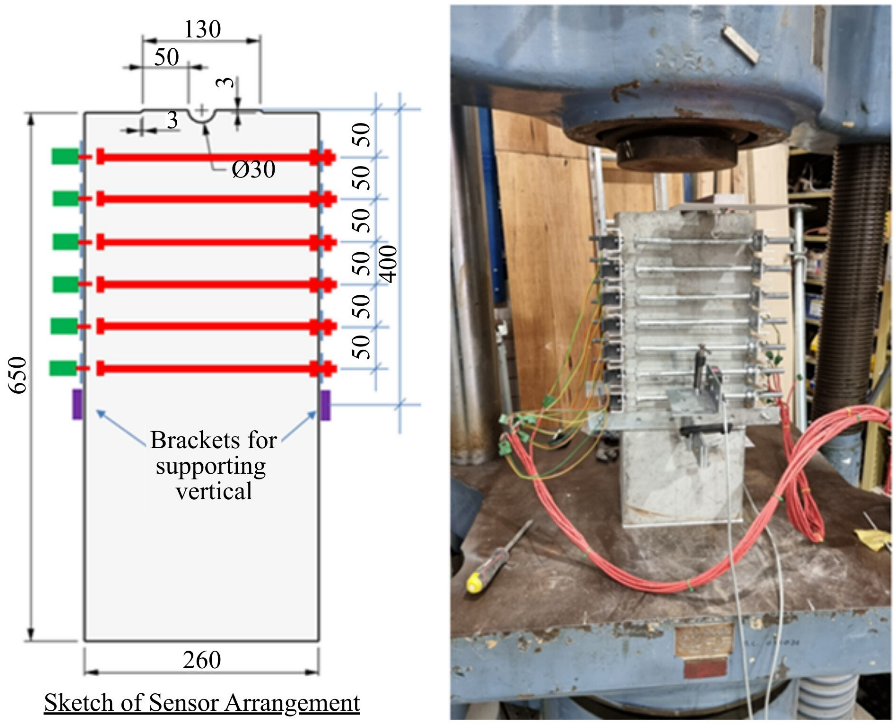

Figure 15. Testing configuration.

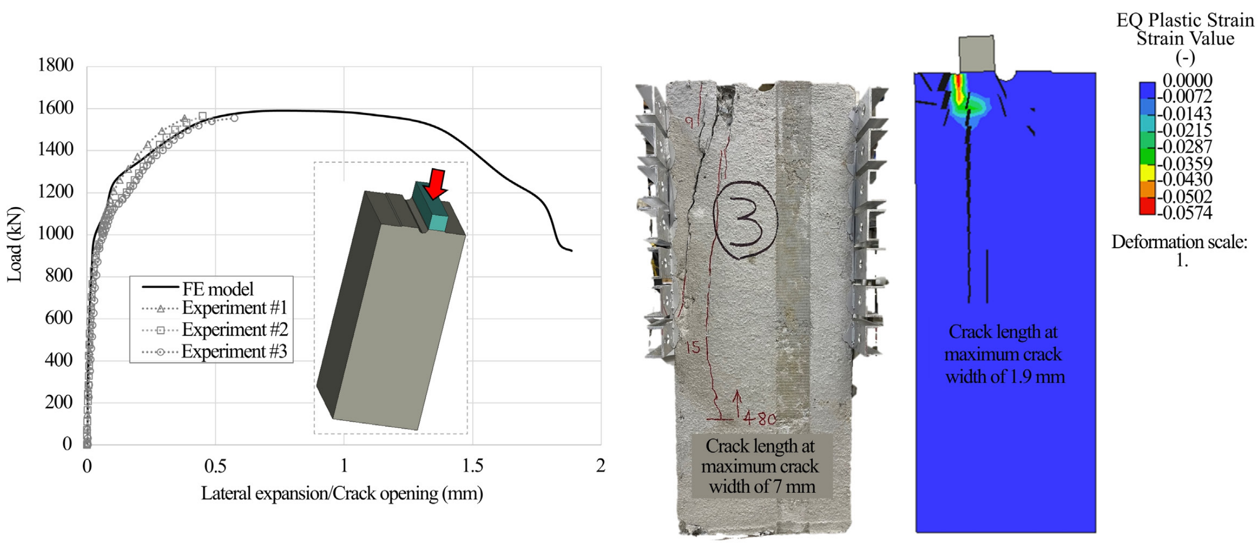

Figure 16. Experimental testing results versus numerical back-analysis: (LHS) load versus crack width curves; (RHS) comparison of cracking pattern between physical samples and numerical model.

Based on the above, sufficient confidence was gained through the non-linear analysis and testing-assisted verification that extra bar reinforcement was not required. This result provided reasonable cost savings and a reduced carbon footprint, and benefited the precast yard by eliminating the need to deal with joint ladder reinforcement, thus slightly improving the casting program.

5. Conclusion

The availability of high-performance steel fibres offers a valuable opportunity for cost-effective, sustainable tunnel lining solutions. By reducing concrete volume and limiting the need for conventional steel reinforcement, Fibre-Reinforced Concrete (FRC) can lower both construction costs and carbon footprint. Additionally, eliminating the need for reinforcement cage placement can shorten construction schedules and improve jobsite safety.

Nevertheless, the full benefits of FRC are often constrained by limitations in conventional design approaches. To unlock its potential, advanced non-linear modelling supported by large-scale field or laboratory testing is essential. As demonstrated by the case studies in this paper, such integrated methods can provide deeper insights and lead to more efficient and reliable tunnel designs.

Acknowledgements

The authors thank the COBRAMSEG 2024 Technical Committee for the invitation to publish the article in Soils and Rocks.

Declaration of interest

The authors have no conflicts of interest to declare. All co-authors have observed and affirmed the contents of the paper and there is no financial interest to report.

Authors' contributions

Tiago de Jesus Souza: data curation, visualization, writing – original draft. David Oliveira: conceptualization, data curation, visualization, methodology, supervision, validation, formal analysis, investigation, project administration, writing – review & editing.

Data availability

The datasets generated and analysed in the course of the current study are available from the corresponding author upon request.

Declaration of use of generative artificial intelligence

This work was prepared without the assistance of any generative artificial intelligence (GenAI) tools or services. All aspects of the manuscript were developed solely by the authors, who take full responsibility for the content of this publication.

List of symbols and abbreviations

f_{ck}	Characteristic value of concrete compressive strength (95% confidence)
f_{cm}	Mean value of concrete compressive strength
f_{ctk}	Characteristic value of concrete uniaxial tensile strength (95% confidence)
f_{R1}	Residual tensile flexural stress capacity at crack mouth opening of 0.5 mm per BS14651
f_{R1k}	Characteristic value of f_{R1} (95% confidence)
f_{R4}	Residual tensile flexural stress capacity at crack mouth opening of 3.5 mm per BS14651
f_{R4k}	Characteristic value of f_{R4} (95% confidence)
CMA	Compressive Membrane Action
CO_{2e}	Embodied carbon
D-Region	Region of disturbed stresses in the concrete
FRC	Fibre-Reinforced Concrete
FRS	Fibre-Reinforced Shotcrete
Q-value	Rock quality index based on rock classification Q-system.
SFRS	Steel Fibre-Reinforced Shotcrete
SLS	Serviceability Limit State
SWTC	Scope of Works and Technical Criteria
TBM	Tunnel Boring Machine
ULS	Ultimate Limit State

References

Barrett, S.V.L., & McCreath, D.R. (1995). Shotcrete support design in blocky ground: towards a deterministic approach. *Tunnelling and Underground Space Technology*, *10*(1), 79-89. https://doi.org/10.1016/0886-7798(94)00067-U.

Bernard, E.S. (2008). Embrittlement of fiber-reinforced shotcrete. *Shotcrete*, *10*(3), 16-21.

Bernard, E.S., Oliveira, D.A.F., & Forrest, B.H. (2022). In situ flexural failure of unbonded fibre reinforced shotcrete linings in response to point loading. *Tunnelling and Underground Space Technology*, *119*, 104235. https://doi.org/10.1016/j.tust.2021.104235.

DAfStb Stahlfaserbeton. (2010). *DAfStb - Guideline — steel fibre reinforced concrete*. Deutscher Ausschuss für Stahlbeton e. V. (In German).

Harding, A. (2022). *Tunnel segmental lining design course notes*. IngeOexpert. Retrieved in July 21, 2025, from https://ingeoexpert.com/en/courses-online/tunnel-segmental-lining-design-course/

International Federation for Structural Concrete - FIB. (2013). *Fib model code for concrete structures 2010*. International Federation for Structural Concrete.

Iyengar, K.T. (1962). Two-dimensional theories of anchorage zone stresses in post-tensioned beams. *ACI Journal Proceedings*, *59*(10), 1443-1466.

Kupfer, H., Hilsdorf, H.K., & Rusch, H. (1969). Behavior of concrete under biaxial stresses. *ACI Materials Journal*, *66*, 656-666.

Leonhardt, F., & Mönnig, E. (1973). *Construções de concreto: casos especiais de dimensionamento de estruturas de concreto armado*. Interciencia.

Menetrey, P., & Willam, K.J. (1995). Triaxial failure criterion for concrete and its generalization. *ACI Structural Journal*, *92*(3), 311-318.

Oliveira, D., & Kozak, P. (2021). A review of the behaviour of domed rock bolt plates and their use in Sydney tunnelling. *Australian Geomechanics*, *56*(3), 73-84.

Oliveira, D.A.F. (2020). *Ground Support for tunnels in Rock*. IngeOexpert. Retrieved in July 21, 2025, from https://ingeoexpert.com/en/courses-online/ground-support-for-tunnels-in-rock/